The Fascicle Undulation Effect on the Activating Function in Magnetic Stimulation of Peripheral Nerves with Transverse and Longitudinal Fields

Eugen R. Lontis[1,*], Karsten Nielsen[2] and Johannes J. Struijk[1]

[1]*Center for Sensory-Motor Interaction SMI, Department of Health Science and Technology, Faculty of Medicine, Aalborg University, Denmark*

[2]*Institute of Pathology, Aalborg Hospital, Denmark*

Abstract: Analysis of activating function for a long, myelinated nerve fiber with undulating path in transverse and longitudinal induced electric fields was performed. The induced electric field was computed using a finite element model composed by a round coil beneath a bath with saline solution. Longitudinal and transverse components of the induced electric field were computed along two axes, one tangential and the other axial to the coil. The influence of a transverse field on the modified activating function was analyzed when the fiber path was determined by the fascicle undulation, and by the fascicle undulation plus the fiber undulation inside the fascicle. For the first path type, undulation wavelength of 40 to 90 mm and 0.8 mm amplitude determined a classic activating function with: (a) multiple virtual cathodes that could generate two or three stimulation sites for axially oriented coil, and (b) virtual cathode with distorted shape in amplitude up to 35% and location up to 67% for tangentially oriented coil. For axially oriented coil, the transverse field term of the modified activating function was comparable in amplitude with the classic activating function, however significant attenuation could occur due to perineurium. For the second path type with wavelength of tenths of millimeters and amplitudes of a quarter of the wavelength, the classic activating function had such a dramatic increase in the spatial frequency that could not predict the stimulation site with the usual interpretation of the virtual cathode. Similarity between the results obtained with the first path type and the ones obtained in a previous in-vitro experiment suggests that the undulating fascicles within the nerve trunk can be responsible for stimulation with transverse fields.

Keywords: Transverse field activation mechanism, Modified activating function, Fiber and fascicle undulation.

INTRODUCTION

Magnetic stimulation has proven to be a valuable technique for diagnostic of the peripheral nervous system. Effective diagnosis, however, requires precise determination of the stimulation site. Models of interaction between the induced electric field and the membrane of the nerve fiber have been analyzed [1-10]. For long nerve fibers within a peripheral nerve trunk, the classic cable theory has arrived at the conclusion that the longitudinal component of the electric field along the fiber path leads to activation, initiated at the negative peak of the longitudinal spatial derivative of the longitudinal field [6, 11-12]. However, experimental observations have led to the conclusion that the transverse field can be responsible for stimulation of the peripheral nerve trunk in inconsistent coil positions, where the electric field has only a transverse component relative to the nerve trunk [13]. Based on these observations and on simulations of cylindrical fibers stimulated electrically [14, 15], Ruohonen *et al*. [13] has adapted the transverse field

activation mechanism to magnetic stimulation, defining the modified activating function. According to this mechanism, depolarization and hyperpolarization of opposite faces of the fiber occur and the stimulation site in this case corresponds to location of the maximum of the transverse field along the fiber.

The fiber undulation inside the fascicle [16-18] has been suggested as an alternative to the transverse field activation mechanism [19-21]. Projection of the transverse field on the wavy fiber path leads to a longitudinal component with a gradient strong enough to produce stimulation, preserving the classic form of the activating function [19]. Another alternative is the inhomogeneity of the surrounding tissue [22]. At the interface between two media of different conductivity, the induced electric field is distorted. Hence, a longitudinal component of the electric field can be generated relative to the nerve fiber, leading to stimulation. Nerve fiber bending can also lead to a higher gradient of the longitudinal field along the nerve fiber at the bending site that can trigger an action potential [23-24].

In a previous *in-vitro* experiment we have analyzed the stimulation sites and thresholds obtained with transverse and longitudinal induced electric fields

*Address correspondence to this author at the Center for Sensory-Motor Interaction SMI, Department of Health Science and Technology, Faculty of Medicine, Aalborg University Fredrik Bajers Vej 7 D3 (A2-203) DK-9220 Aalborg, Denmark; Tel: +45 9940 2435; Fax: +45 9815 4008; E-mail: lontis@hst.aau.dk

applied with a round coil along a straight phrenic nerve of pig, in the absence of surrounding inhomogeneous tissue [25]. The aim of the experiment was to differentiate between the classic activation mechanism, denoted as longitudinal field activation mechanism that is based on the gradient of the longitudinal component of the induced electric field, and the transverse field activation mechanism in the analysis of the stimulation site. Coil oriented tangentially has generated a bell-shaped longitudinal field along the nerve trunk, with a maximum corresponding to the coil center. In addition, a biphasic transverse field with modulus maxima located at approximately one radius symmetric to the coil center has been generated with approximately 30% lower amplitude. A constant stimulus applied along the nerve trunk in successive positions of the coil tangentially oriented has determined a stimulation site in the vicinity of the maximal negative gradient of the longitudinal field, as predicted by the cable theory. However, threshold variations without unchanged latency of the recorded compound action potential CAP (*i.e.* hot spots) have been noticed. Furthermore, distortion of the CAP shape similar to overlapping responses from two stimulation sites has been recorded in approximately 10% of the cases. Coil oriented axially has generated solely a transverse induced electric field of same maximal amplitude along the nerve trunk as the longitudinal induced electric field generated when the coil has been tangentially oriented. For coil axially oriented, the shape of the compound action potential has suggested one, two or three sites for the action potential initiation. The pattern of these sites has varied as well with the coil position along the nerve trunk. Two distinct types of two stimulation sites pattern have been noticed. For one type, the stimulation sites have been relatively close to the location of the two absolute maxima of the transverse electric field, supporting the site prediction by the transverse field activation mechanism. The other type has been characterized by distanced stimulation sites (scattered) relative to the field maxima. The three sites pattern has had the central site closed to the coil center, where the transverse electric field has had zero amplitude and maximal spatial derivative along the nerve trunk, whereas the two outer sites have been distanced around the location of the two absolute maxima of the transverse field, contrary to the site prediction by the transverse field activation mechanism.

These experimental observations, combined with anatomical knowledge, have suggested that the stimulation due to the transverse field is dependent on the nerve trunk structure, in particular to the fascicle undulation. Sunderland, in a review of the peripheral nerve structure [26], has outlined that histological analysis performed on consecutive cross-sections shows that the size, number, and location of the fascicle depend on the sampling location along the trunk, which has been also shown in the pig phrenic nerve [25]. The network of fascicles that form fascicular plexuses, with a spatial frequency in the order of centimetres, generates fascicular undulation.

In this simulation study, an analysis of the modified activating function for a path of a nerve fiber defined by the fascicular and fiber undulations in longitudinal and transverse induced electric fields has been performed. The aim of the study is to evaluate if the induced electric field along the fiber path generates enough gradient that can lead to stimulation according to the longitudinal field activation mechanism due to undulations of the fibers within undulating fascicles of a nerve trunk, as compared to the transverse field activation mechanism, in order to explain the experimental findings mentioned above. Differentiating the effects of the longitudinal and transverse induced electric fields in determination of the stimulation site and threshold plays a major role in the effective coil design for magnetic stimulation techniques for diagnosis of the nervous system.

1. METHODS

The induced electric field along the path of the fiber and the cable equation were used in computation of the activating function. Computation of the induced electric field attempted to reproduce the previous in-vitro experimental set-up and stimulation [25], however, without considering the structure of the nerve trunk. Although the nerve trunk structure can distort the electric field along the fiber path, it is common in practice to use the electric field along a long peripheral nerve trunk as input in the cable equation in order to estimate the site of stimulation. The present study analyzed solely the effect of the undulation of the fiber path on the activating function based only on the projection of the induced electric field along the nerve trunk (*i.e.* axis of computation) on the path of the fiber. A finite element model computed the induced electric field along an axis of computation tangential or axial relative to a round coil in a bath with saline solution, above the coil (Figure **1a**). This computed induced electric field was regarded as 'the field along a nerve trunk'. Projecting this field on the fiber path resulted in longitudinal and transverse components used as input in the cable equation.
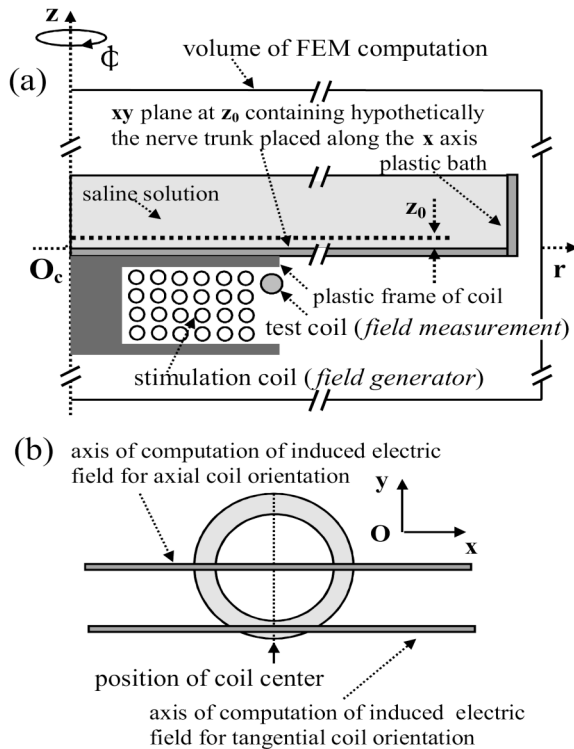
Figure 1: (**a**) Finite element model of the saline bath and stimulation coil, with rotational symmetry in cylindrical coordinate system **rzϕ**, not to scale. (**b**) Axis of computation of the induced electric field for axial and tangential coil orientations, in the **xy** plane at $z_0 = 1$ mm above the bottom of the bath, seen from above.

## 1.1. Finite Element Model for Computation of the Induced Electric Field

A bath filled with saline solution was simulated as a cylinder with a radius of 125 mm and a height of 30 mm, with 3 mm thick plastic walls (Figure **1a**). The stimulation coil had an inner and outer radius of 15 and 25 mm, respectively, a height of 8 mm and 24 windings with 1.6 mm copper wire, build on a plastic frame. The plastic frame added a distance of 1 mm between the bath's bottom and the nearest winding. A test coil, with a radius of 26 mm, 0.4 mm copper wire and a single winding around the stimulation coil, was used to calibrate the stimulation pulses. The volume of computation was a cylinder with a radius of 150 mm and a height of 140 mm. Electrical parameters of materials, relative permittivity ε_r and conductivity σ, used in the model were as follows: $\varepsilon_r = 1$ and $\sigma = 0$ S/m for air, $\varepsilon_r = 40$ and $\sigma = 1.5$ S/m for saline solution, $\varepsilon_r = 4.5$ and $\sigma = 0$ S/m for plastic, and $\varepsilon_r = 1e^{10}$ and $\sigma = 5.99e^7$ S/m for copper. All materials were considered diamagnetic with relative magnetic permeability $\mu_r = 1$.

Preliminary simulations showed that a current with a rate of 57 A/μs induced the same maximum voltage of 24.5 V in the test coil as obtained experimentally, at 90% of maximum stimulator output with a measured current rate of 59 A/μs. All computations referred to this stimulus intensity. Comparison between the activating function magnitudes and the threshold values obtained experimentally could be performed due to the linear relations between the stimulator output and the current rate, and the activating function and the current rate, respectively.

The induced electric field along a tangential and axial axes of computation relative to the coil (Figure **1b** top view, in a plane **xy** at $z_0 = 1$ mm from the bath's bottom) was used in computation of the longitudinal and transverse components of the electric field along the fiber path (Figure **2** and Figure **3**).
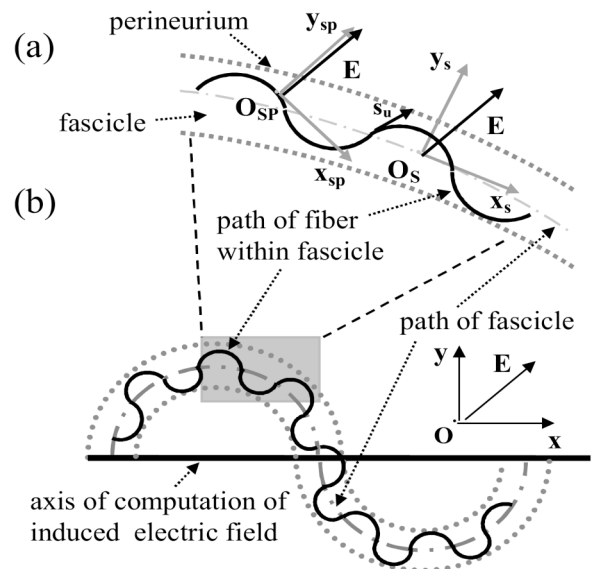
Figure 2: (**a**) Segment of a fiber path determined by the fascicle and fiber undulations. Rectangular coordinate systems $x_{sp}y_{sp}$ and $x_s y_s$, relative to fiber path and to fascicle, on which projections of the electric field E are computed. Rectangular coordinate system xy of the coil from Figure **1b**. (**b**) Fiber path composed by the fascicle undulation and fiber undulation.

1.2. Field Equations

The current through the coil (of density $\mathbf{J}^e$) and the induced electric current (of density $\mathbf{J}_i = \sigma\, \mathbf{E}$, where $\mathbf{E}$ was the induced electric field) generated a magnetic field with intensity $\mathbf{H}$, according to Ampere's law $\nabla \times \mathbf{H} = \mathbf{J}_i + \mathbf{J}^e$. This equation was valid under the quasistatic approximation, according to which the electromagnetic field does not propagate at the frequencies used in magnetic stimulation (*i.e.* no displacement currents present) [27]. Electric and
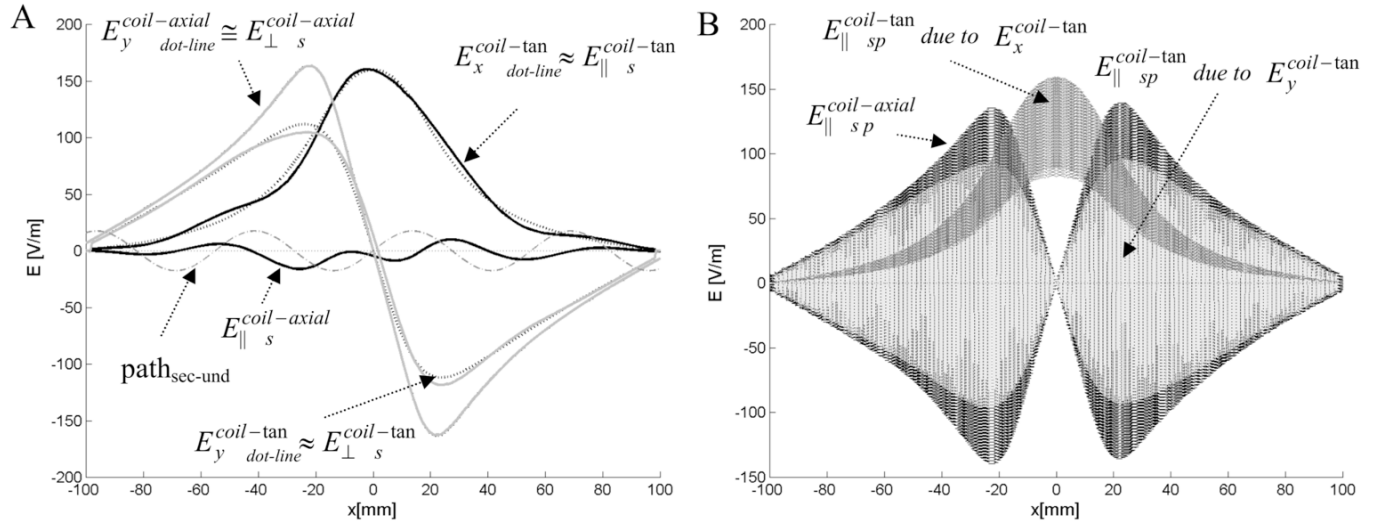
Figure 3: Induced electric field (E_x and E_y components in coil reference system **xy**) and projections ($E_{\parallel}$ and $E_{\perp}$ components in path reference system **$x_s y_s$** or **$x_{sp} y_{sp}$**) on the fibre path determined by: (**a**) Fascicle undulation (*s* secondary) with λ_s=55mm and A_s=0.8 mm, and (**b**) Same as (**a**) plus the fibre undulation (*p* primary) with λ_p=0.55mm and A_p=0.125 mm.

magnetic fields could be expressed as functions of magnetic **A** and electric V potentials, according to: $\mathbf{E} = -\nabla V - \dfrac{\partial \mathbf{A}}{\partial t}$ and $\mathbf{B} = \nabla \times \mathbf{A}$. Using the constitutive equations: $\mathbf{D} = \varepsilon_0 \mathbf{E} + \mathbf{P}$ and $\mathbf{B} = \mu_0 (\mathbf{H} + \mathbf{M})$ the Ampere's law could be rewritten for a nonhomogeneous volume conductor as:

$$\sigma \frac{\partial \mathbf{A}}{\partial t} + \nabla \times \left(\mu^{-1} \nabla \times \mathbf{A} - \mathbf{M} \right) + \sigma \nabla V = \mathbf{J}^e \qquad (1)$$

Equation of continuity that expressed the divergence of the total current density $\nabla \cdot \left(\mathbf{J}_i + \mathbf{J}^e \right)$ could be written from equation (1) as:

$$-\nabla \cdot \left(\sigma \frac{\partial \mathbf{A}}{\partial t} + \sigma \nabla V - \mathbf{J}^e \right) = 0 \qquad (2)$$

considering that the divergence of a curl of any vector was zero $\nabla \cdot (\nabla \times \mathbf{H}) = 0$. Solving the set of equations (1) and (2) for variables **A** and V provided a solution for the electric **E** and the magnetic field **H**.

The 3D finite element model of the system composed by the bath, the stimulation and the test coils could be reduced to a 2D model in cylindrical coordinates due to the rotational symmetry around the axis normal to the coil center (Figure **1a**). The $\mathbf{J}^e$ presence along the ϕ direction only implied that the vectors **A** and $\mathbf{J}_i = -\sigma \nabla V$ also had components in the ϕ direction only, A_ϕ and $J_{i\phi}$. The term ∇V vanished because the induced current flowed only in the ϕ direction in a homogenous medium. The time

dependent equation (1) was solved with a finite element method using Femlab 2.0.

The induced electric field was computed in cylindrical coordinates **rz** for a given angle ϕ subsequently transformed into 2D rectangular coordinates **xy** for z_0 = 1 mm (Figure **1a**). The induced electric field at y = 0 mm and y = 20 mm for any x was used to compute the activating function according to the cable equation, in the case of tangentially and axially oriented coil, respectively (Figure **1b**).

1.3. Initial Assumptions

No structure of the nerve trunk was used in computation of the induced electric field. The fiber path 'waved' around the axis of computation of the induced electric field (Figure **1b** and Figure **2b**). Practically this axis could be seen as the positioning line of a nerve trunk in the bath. In any point of the fiber path the electric field varied along the computation axis x only (*i.e.* constant electric field in y direction), considering the very small deviations of the path from the computation axis. Consequently, the electric field at any point on the fiber path was the same as the electric field at the junction point between the axis of computation and the vertical to the point on the fiber path. The attenuating effect of the perineurium was estimated according to the electromagnetic theory for electric fields at the interface between two media of different conductivity [19]. According to this theory, the perineurium of a cylindrical fascicle would attenuate the electric field normal to the fascicle. The fiber run

virtually within a fascicle of constant radius that evolved along the axis of the nerve trunk (*i.e.* axis of computation) defining the fascicle undulation. The addition of the fiber undulation inside the fascicle formed the fiber path relative to the coil reference system.

Two particular geometries for the fiber path were used initially to assess the modified activating function. The wavelengths of the fascicle undulation of 55 and 74 mm were suggested by the threshold variations as function of coil position as observed in two nerve trunks in the previous experiment [25]. These two cases gave the most distinct patterns for the stimulation sites, one supporting the longitudinal field activation mechanism and the other supporting the transverse field activation mechanism, when a transverse field was applied to the nerve trunk with a round coil tangentially oriented. The maximal undulation amplitude of 0.8 mm was chosen with reference to the maximal diameter of the previously mentioned nerve trunks. The fiber undulation within the fascicle had a wavelength of tenths of millimeters and amplitude of a quarter of the wavelength [19, 25].

1.4. Computation of Path and Electric Field Projections

For a better graphical representation of both terms of the modified activating function, the evolution of the fiber path was restricted to the 2D space. The index of both types of undulation were referred as 's' from *secondary* for the fascicle undulation and 'p' from *primary* for the fiber undulation. The paths $\mathbf{s_s}$, $\mathbf{s_p}$ determined by the fascicle and by the fiber undulation, with wavelength λ_s and λ_p, were expressed as

$$s_S = A_s \sin(\frac{2\pi}{\lambda_s} x + \varphi_s) \quad \text{and} \quad s_P = A_p \sin(\frac{2\pi}{\lambda_p} x + \varphi_p),$$

respectively. Since $\lambda_s/\lambda_p \approx 100$ and $A_s/A_p \approx 10$ were used in simulation, the path $\mathbf{s}$ composed by both fascicle and fiber undulations was approximated as $\mathbf{s_{sp}}$ = $\mathbf{s_s}$ + $\mathbf{s_p}$. In this way the path $\mathbf{s_{sp}}$ was a functional of x, and a point on the discrete x axis had a unique corresponding point on the path $\mathbf{s_s}$ and $\mathbf{s_{sp}}$, respectively. This approach helped in the interpretation of the equivalence in the path integration along $\mathbf{s_s}$ and $\mathbf{s_{sp}}$.

In Figure **2a**, a path segment is shown in the **xy** plane at z_0. The coordinate systems $\mathbf{x_s y_s}$ and $\mathbf{x_{sp} y_{sp}}$ relative to the $\mathbf{s_s}$, $\mathbf{s_p}$ paths were defined. The electric field projections were determined on these coordinates systems for an arbitrary point along each path. These points were on the same vertical to x axis. The electric

field projections $\mathbf{E_{sp}}$=[$E_{\perp sp}$ $E_{\| sp}$]' on the path $\mathbf{s_{sp}}$ and $\mathbf{E_s}$=[$E_{\perp s}$ $E_{\| s}$]' on the path $\mathbf{s_s}$ were computed according to assumption of constant field along the computational axis as:

$$\mathbf{E_{sp}} = R_d R_s \mathbf{E} \quad \text{and} \quad \mathbf{E_s} = R_s \mathbf{E} \tag{3}$$

respectively, where $\mathbf{E}$=[E_y E_x]' was the electric field in the **xy** reference system of the stimulating coil. The rotation matrices were given by

$$R_s = \begin{bmatrix} \cos(\theta_s) & -\sin(\theta_s) \\ \sin(\theta_s) & \cos(\theta_s) \end{bmatrix}$$

$$\text{and} \quad R_d = \begin{bmatrix} \beta\cos(\theta_d) & -\sin(\theta_d) \\ \beta\sin(\theta_d) & \cos(\theta_d) \end{bmatrix}.$$

The attenuation of the perineurium was simulated by the factor β. The spatial derivative of the path determined the tangent of the path angle. Consequently, the angle of the path was:

$$\theta_s = \operatorname{atan}(\frac{\partial s_s}{\partial x}) \quad \text{and} \quad \theta_{sp} = \operatorname{atan}(\frac{\partial s_{sp}}{\partial x}) \tag{4}$$

for $\mathbf{s_s}$ and $\mathbf{s_{sp}}$, respectively, with $\theta_d = \theta_{sp} - \theta_s$.

1.5. Cable Equation

The differential form for the passive steady state model of the myelinated nerve fiber was obtained from the compartmental cable equation [6, 28] by removing the capacitive current. The myelin sheath was assumed a perfect insulator. The transverse induced electric field $E_\perp$ was introduced in the right side of the cable equation by the modified activating function [13], as shown below:

$$\lambda^2 \frac{d^2 V_m(s)}{ds^2} - \left(V_m(s) - E_L\right) = \lambda^2 \left(a(s) - \frac{d}{\lambda^2} E_\perp\right) \tag{5}$$

where $V_m(s)$ was the transmembrane potential along the fiber path s, E_L the resting potential, and $\lambda = \sqrt{\dfrac{d}{4\rho_a g_L} \dfrac{\Delta s}{l}}$ was the space constant. The path of the nerve fiber was described by the unity vector $\mathbf{s_u}$ in the 3D Euclidian space **xyz** (Figure **2**). The fiber with diameter d of 10 μm, internodal distance Δs of 0.6 mm and nodal width l of 1.5 μm had an axoplasmic resistivity ρ_a of 57.4 Ωcm and a leakage conductance g_L of 128 mS cm^{-1}. The classic activating function $a(s)$ was expressed at node n as:

$$a(n) = \frac{\Delta E_\parallel}{\Delta x} = \frac{\int_{s(n)}^{s(n+1)} E_\parallel ds - \int_{s(n-1)}^{s(n)} E_\parallel ds}{\Delta s^2} \qquad (6)$$

where $E_\parallel$ was the longitudinal component of the induced electric field along the nerve fiber path. Depolarization occurred where the activating function was negative. In order to compare the effect of the transverse field relative to the classic activating function, the following term was used:

$$a_{m(n)} = a(n) - \frac{\mathrm{d}}{\lambda^2} E_\perp \qquad (7)$$

as an expression for the modified activating function evaluated at node n. The transverse field's additional term, evaluated at node n, was:

$$tfat(n) = \frac{\mathrm{d}}{\lambda^2} E_\perp \qquad (8)$$

The effect of the perineurium was evaluated for up to 10 times attenuation between the intra and extra-fascicular transverse component of the induced electric field.

2. RESULTS

2.1. Induced Electric Field and its Projections on the Fiber Path

Longitudinal E_x and transverse E_y components of the induced electric field for both coil orientations and projections longitudinal to the path $\mathbf{s_s}$, with a wavelength λ_s of 55 mm and amplitude A_s of 0.8 mm, are shown in Figure **3a** without perineurium attenuation. For tangential coil orientation, E_x had a maximum of 163 V/m at the coil center and a derivative with maximal modulus of 4.25 kV/m² at ± 18 mm from the coil center. For axial coil orientation, E_x was zero and E_y had the same maximal modulus of 163 V/m, located at ± 22 mm from the coil center. E_y along the nerve trunk for tangential coil orientation was similar to E_y for axial coil orientation, attenuated with 1.56. Projection $E_{\perp\,s}$, transverse to the path, was practically the same with the transverse field component E_y for both coil orientations. Addition of the fiber undulation, with a wavelength λ_p of 0.5 mm and amplitude A_p of 0.125 mm, drastically modified the resulting projection by amplitude modulation for both coil orientations (Figure **3b**).

### 2.2. Fiber Path Determined by Fascicle Undulation

The classic activating function term *a(n)* from equation (7) for the two particular geometries of the

fiber path, λ_s of 55 and 74 mm, and phases φ_s of zero, $\pi/2$, π and $3\pi/2$, is shown in Figure **4a** for both coil orientations. Additionally, the transverse field's term *tfat(n)* from equation (7) is represented only for the path phase φ_s of zero, without perineurium attenuation ($\beta = 1$). Moving the coil to the right along the nerve trunk was equivalent to an increase in the undulation phase when the coil was fixed.

For axial coil orientation, only E_y projection on the path contributed to *a(n)* as E_x was zero (Figure **4a**), resulting in an *a(n)* with multiple virtual cathodes (local minima). Amplitude of *a(n)* was linear with the E_y amplitude and almost linear with the path amplitude for a relative small variation of the path's angle. Location of the virtual cathodes, for a given E_y, was highly dependent on the path phase. Consequently, for λ_s of 55 mm and phase φ_s of zero, *a(n)* had three local minima with the one in the middle corresponding to the coil center, having the lowest amplitude (Figure **4a**, left). As the phase shifted from zero to π, *a(n)* was symmetrical relative to *x* axis, having four local minima, where the two outermost were approximately half in amplitude as compared to the two closer to the coil center. A path with a phase of $\pi/2$ shifted *a(n)* towards left, relative to phase zero. This shift resulted in a non-uniform change of *a(n)* amplitude, increasing from right to left. This could generate nerve responses with the same latency for two different coil positions. The path with a phase of $3\pi/2$ mirrored *a(n)* given by the path with a phase of $\pi/2$.

At the sites corresponding to a maximum in absolute value of the transverse field (± 22 mm from coil center) *a(n)* had two local minima of 1.72 kV/m² in absolute value, for a path phase of π. For λ_s of 74 mm, the modulatory effect of the path on *a(n)* was similar to the λ_s = 55 mm case (Figure **4a**, left). However due to a greater wavelength, the locations of the virtual cathodes were further away from the coil center, resulting in a lower number within the same *x* axis window and a smaller amplitude of the virtual cathodes. For a path phase φ_S of π, only two local minima were present as compared with the four local minima, as in the case of 55 mm wavelength. For λ_s of 74 mm, the two local minima of *a(n)* at ± 22 mm from coil center had 1.12 kV/m² in absolute value, at a path phase between π and $3\pi/2$.

For tangential coil orientation in the absence of path undulation, only E_x contributed to *a(n)* that had a computed absolute maximum of 4.25 kV/m² at ± 18 mm from the coil center. The modulatory effect of the
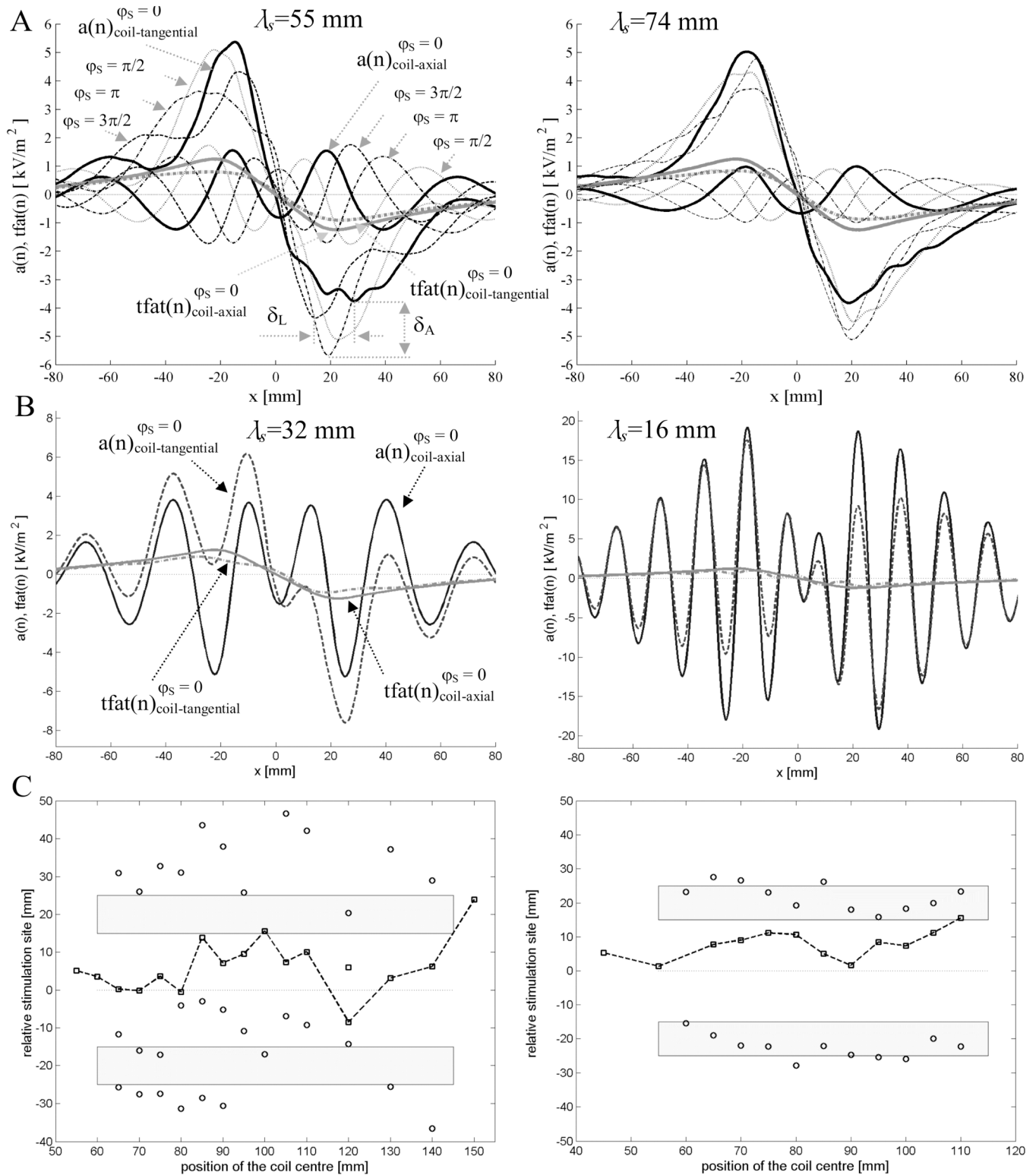
Figure 4: (**a**) Modified activating function terms a(n) and tfat(n) for a fiber path given by the fascicle undulation with parameters: path phase $\varphi_S = 0$ to $3\pi/2$, amplitude $A_s = 0.8$ mm, wavelength $\lambda_s = 55$ mm (left), $\lambda_s = 74$ mm (right) and internodal distance $d_n = 0.6$ mm, without perineurium attenuation. (**b**) Same as (**a**) for path phase $\varphi_S = 0$ and wavelength $\lambda_s = 32$ mm (left), $\lambda_s = 16$ mm (right). (**c**) Estimates of the stimulation sites relative to the coil center position previously obtained experimentally on phrenic nerves of pig (left, nerve no. 1 and right, nerve no. 5); the round coil had an inner and the outer radius of 15 and 25 mm, respectively, delimited by the shadow blocks. Squares and dashed line represents the relative stimulation sites for the coil oriented tangentially and circles for the axial coil orientation.

path was present on both E_x and E_y, when the path was defined by the fascicle undulation. This effect was smaller for the longitudinal component E_x than for the transverse component E_y, since it was given by multiplication with the sine and cosine of the path's angle, respectively, for a given coil orientation. For the same angle around zero, the sine produced a greater variation than the cosine. For tangential coil orientation, the effect of the transverse field E_y was similar to the one with the coil in axial orientation, however attenuated with 1.56 (ratio factor between the spatial distributions of the transverse field in the two coil orientations). Both these effects were included in the shape of *a(n)* that could determine a variation in the amplitude δ_A and location δ_L of the local minimum that defines the virtual cathode (Figure **4a**, left). These variations were dependent on the undulation wavelength, with ranges δ_A of 3.6 to 5.8 and 3.85 to 5.2 kV/m^2, and δ_L of 12 to 30 and 18 to 21 mm for λ_s of 55 and 74 mm, respectively.

The transverse field term *tfat(n)* computed from $E_{\perp s}$ was comparable with *a(n)*, with respect to the maximal magnitude of 1.25 kV/m^2 for axially oriented coil. For λ_s of 55 and 74 mm, the path had no obvious effect on *tfat(n)*, since this term was proportional to the magnitude of the transverse field projection to the path and not to its gradient, according to equation (8). $E_{\perp s}$ was practically the same as E_y, with a minor contribution of E_x. For tangential coil orientation *tfat(n)* was attenuated with 1.56.

In Figure **4c**, the stimulation sites relative to the coil center are plotted for both coil orientations as obtained experimentally [25] from two phrenic nerves, with an effective nerve length (measured from the cuff electrode) of 172 and 140 mm, respectively. Similar to these experimental results, patterns of three and two stimulation sites for the axial coil orientation when the phase of the path increased (*i.e.* the coil moving along the nerve trunk) could be generated by *a(n)* as in Figure **4**. The length of the nerve trunk along which the coil was moved was important for a given undulation wavelength. For λ_s of 55 mm only in the vicinity of phase π, a stimulation threshold high enough could rule out the two outermost virtual cathodes and preserve the two innermost that could initiate an action potential (Figure **4a**, left). In this case, a two stimulation sites pattern could be obtained, and for another path phase three stimulation sites were likely to occur. In contrast, for λ_s of 74 mm (Figure **4a**, right), the three stimulation sites pattern was more restricted to the vicinity of phase zero. Outside the vicinity of phase zero, however, a pattern of two stimulation sites could be

most common, relatively close to the location of the maximal transverse field E_y modulus. In the vicinity of the maximum of the transverse field, a pattern of two stimulation sites could be obtained along the nerve, if the coil position was further away from the phase zero.

The ratio of the magnitude of the virtual cathodes R_{VC} was within 2.2 to 5.6 and 3.4 to 5 for λ_s of 55 and 74 mm, respectively, for tangential and axial coil orientation. R_{VC} was in the order of the samples obtained experimentally that had a lower value between 1.7 to 3.8 and an upper value between 2.8 to 5.4.

In Figure **4b**, the terms *a(n)* and *tfat(n)* of the modified activating function $a_m(n)$ are plotted similar to those from Figure **4a** for λ_s = 32 and 16 mm, respectively. An increasing effect of the path modulation of E_y relative to E_x on the *a(n)* amplitude was noticed, for tangential coil orientation. For λ_s of 32 mm, the modulation imposed by the path determined three local minima in *a(n)* that could lead to a compound action potential with multiple peaks. A further decrease in λ_s to 16 mm showed a dominant influence of E_y modulation. Besides the increase in the number of the local minima, the *a(n)* envelope approximated the shape of the E_y modulus. The *tfat(n)* term remained almost unchanged in comparison with the great change in the *a(n)*.

2.3. Path Determined by Fascicle and Fiber Undulations

In Figure **5**, the activating functions are shown for undulating fiber paths composed by both the fascicle undulation and the fiber undulation within the fascicle. The trend observed when the path was determined by the fascicle undulation only for wavelength below 32 mm was also visible in the case of the path defined by fascicle undulation, with λ_s of 55 mm and A_s of 0.8 mm, plus fiber undulation, with λ_p of 0.55 mm and A_p of 0.125 mm, and no perineurium attenuation β = 1 (Figure **5**, left). Addition of fiber undulation yielded the same type of shape of *a(n)* for both coil orientations, with higher amplitude for axial than for tangential coil orientation, as in Figure **4b** for axial coil orientation. However, a higher spatial frequency was imposed by the fiber undulation. The overall shape of *a(n)* was similar to that of the longitudinal projection $E_{\parallel sp}$ of E_y to the path (Figure **3b**). The transverse field term *tfat(n)* is plotted in Figure **5b**, left, and it had a relatively small maximum amplitude. Its effect added to *a(n)* was negligible, for the given path geometry.
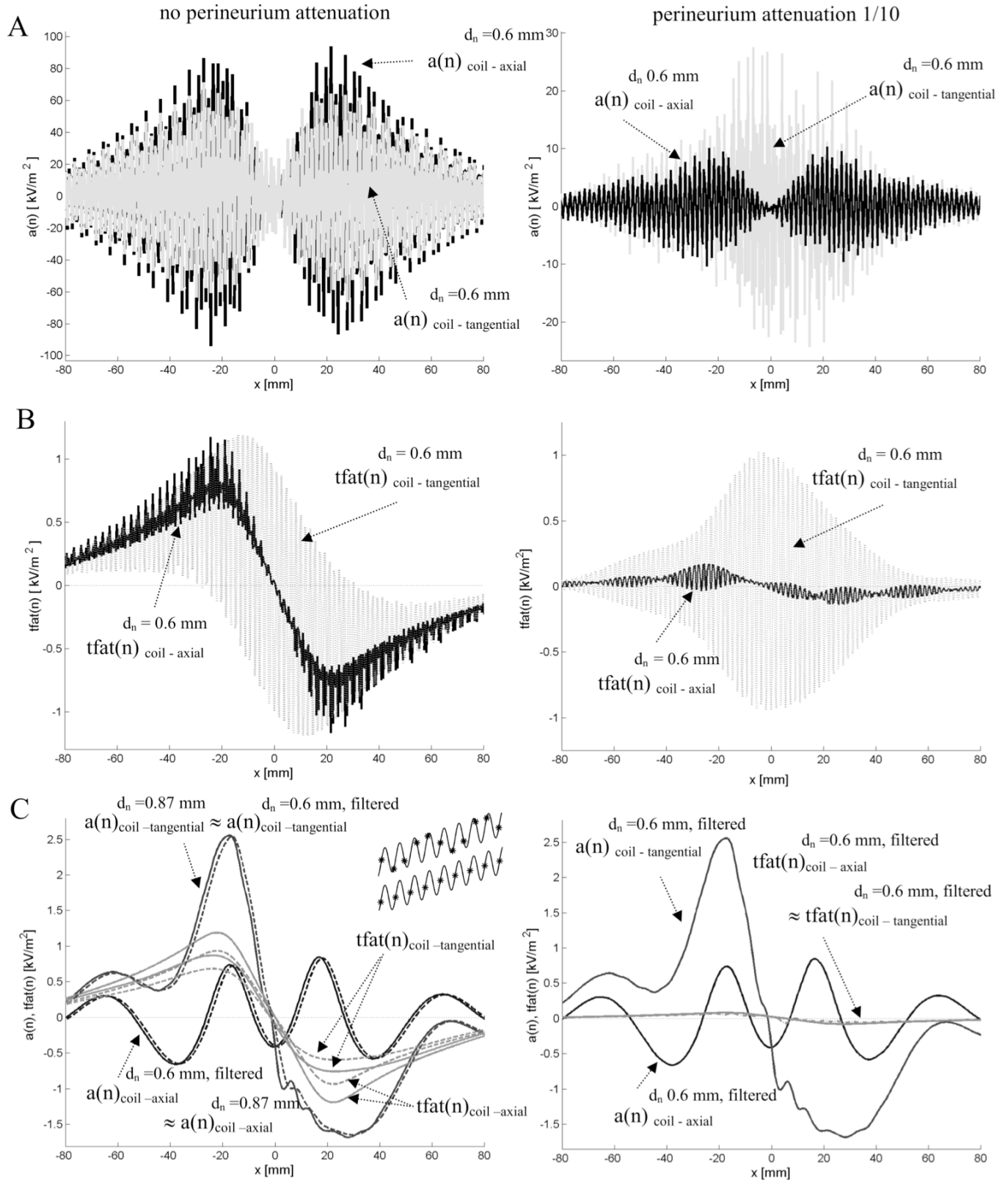
Figure 5: Modified activation function terms a (n) and tfat (n) for a fiber path given by the both fascicle (λ_s=55 mm, A_s=0.8 mm) and fibre (λ_p=0.55 mm, A_p=0.125 mm) undulations and internodal distance d_n =0.6 mm, without (left) and with perineurium attenuation (right). (**a**) Classic activation function a(n). (**b**) Transverse field's additional term tfat(n). (**c**) Filtered version (solid line) of a(n) and tfat(n) terms from (**a**) and (**b**), and additional the case of the fibre with d_n=0.87 mm (not filtered, left, dashed line).

If the internodal distance d_n increased from 0.6 mm to 0.87 mm, the nodes were almost aligned with the path given by the fascicle undulation (inset Figure **5c**, left), and the *a(n)* had an almost identical shape with that of *a(n)* computed with the internodal distance of 0.6 mm and filtered (Figure **5c**, left). Consequently, the shape of *a(n)* in Figure **5a** was defined by the effect of the fascicle undulation, to which was added the effect of the fiber undulation in the form of a high spatial frequency shape modulated in amplitude by the E_y. The effect of fiber undulation within the fascicle on the shape of *a(n)* was proportional to the degree of node alignment with the path defined by the fascicle undulation. The *tfat(n)* term was also modulated by the path, but to a less extent than *a(n)*.

Due to the superimposed fascicle undulation effect (*i.e.* the filtered *a (n)* from Figure **5c**, left), the *a(n)* for a fiber path defined by the fiber and fascicle undulations was proportional to the *a(n),* when the fiber path was defined by the fascicle undulation (Figure **4a**). The proportionality factor α_a was the ratio between the length of the equivalent path between the node along the fascicle undulation path and the internodal distance d_n, with a value α_a of 0.48 for the case presented. The integral difference in (6) was the same for any path of the electric field integral since the voltage between two points was the same for any path integral. If the equivalent fascicle undulation effect was to be assessed, the new equivalent internodal distance d_n = $0.6*\alpha_a$ = 0.29 mm along the fascicle undulation path should be used, instead of the current internodal distance 0.6 mm along the fascicle and fiber undulation path. The same was valid for *tfat(n)*, but the proportionality factor was given by α_a = 0.69 due to the fiber space constant λ that was dependent on the internodal distance. The *tfat(n)* computed in the case of an internodal distance of $1.46*0.6$ mm differed from the *tfat(n)* obtain through filtering because of the imperfect node alignment and, thus, extra modulation was added (Figure **5c**, left).

The perineurium attenuation, with the factor β = 0.1, reduced E_y 10 times and thus reduced its contribution to *a(n)* for both coil orientations (Figure **5**, right). Contribution of E_x to *a(n)* in the tangential coil orientation became more visible in the form of an envelope defined by the shape of E_x from Figure **5a**. When perineurium attenuation was simulated, the spatial filtering of *a(n)* showed that the fascicle undulation effect on *a(n)* remained unchanged, but decreased the *tfat(n)* (Figure **5c**, right).

3. DISCUSSION

3.1. Transverse vs. Longitudinal Induced Electric Field. Projections on Undulating Fiber

The classic activating function, computed under simplifying assumptions (see methods) along a 10 μm fiber with a path defined by the fascicle undulation only, may explain why the transverse field can lead to fiber stimulation through the gradient of its projection on the fiber path. Assuming an undulation wavelength between 40 and 90 mm, the simulated stimulation sites patterns and the ratio between the stimulation thresholds in the two coil orientations are close to the ones obtained experimentally [25]. If the coil movement along the nerve avoids the region with path phase φ_S of zero and when the undulation wavelength is above 70 mm than prediction of the stimulation sites is very close to that of the transverse field mechanism theory [13]. This theory states that the stimulation site corresponds to the location of the maximum of the field and not to its gradient, when only a transverse field is applied along the nerve fiber.

The additional term given by the transverse field, introduced in the modified activating function according to the transverse field mechanism theory, has a magnitude that is comparable with that of the classic activating function when the coil is axially oriented and it can contribute to stimulation. This contribution is much attenuated if the perineurium shielding effect is taken into account [19]. However, the addition of the fiber undulation inside the fascicle considerably distorts the classic activating function, both in amplitude and spatial frequency. The additional term is also distorted in the spatial frequency but much less in amplitude, so the contribution to the modified activating function is minor. In this case, the usual interpretation of the virtual cathodes in the classic activating function cannot be applied properly to predict the stimulation sites.

Theoretically, the modulatory effect of the fiber undulation can be canceled if the nodes are aligned with the path defined by the fascicle undulation, but this is valid only for a particular ratio between the fiber undulation wavelength and internodal distance. However, the node alignment effect is less likely to work in practice, since the fiber undulation is not constant throughout the nerve length as exemplified for the pig phrenic nerve [25], and it cannot provide the constant ratio required.

3.2. Critique of Methodology

The experimental results obtained in the previous study [25] cannot be fully explained by the

computations presented under the simplifying assumptions assumed in this study. The finite element model for field computation must include the nerve trunk in the volume conductor for a more realistic interpretation of the effect of the perineurium of the twisted fascicular network. One may suggest that the highly insulated myelinated nerve fibers, which in the particular case of the pig phrenic nerve are of relative constant diameter and tightly packed in the fascicle [25], maintain in the axoplasm of the fiber within the fascicle an electric field longitudinal to the fascicle. This would preserve all the observations made in the analysis of the activating function when the path is defined by the fascicle undulation only. However, this issue cannot be stated conclusively and further analysis of the induced electric field inside the nerve trunk must be performed. The model presented cannot directly discriminate between the modulatory effect of the fiber and fascicle undulations in computation of the activating function.

Results based on relatively simple models of field computation must be carefully evaluated. Due to rotational symmetry, the current flows in the φ direction crossing no interface between two media. If this condition of current flow is not respected during an experiment, charge accumulations occur at the interface between two media of different conductivities [29-31]. The field distribution along the nerve trunk or fiber changes with possible consequences on the analysis of the activating function.

The fiber undulation inside the fascicle has been well documented in the literature [26, 32, 33]. Fiber undulations can be easily visible in the histological analysis of a cross section of a nerve trunk. Sunderland [26] has analyzed the fascicle undulation mainly for branching peripheral nerve trunks. Fascicular plexuses are formed where fascicles converge and diverge, their presence being suggested by the need of fiber relocation required by a branching point. This phenomenon exists, however, in the case of non-branching peripheral nerve as the phrenic nerve. The fascicular plexus forms at relative short distance, in the order of centimeters. The nerve fibers belonging to a branch are found proximal along the trunk grouped at different location inside the successive cross-sections, resembling a wavy trajectory with wavelength in the order of centimeters that is consistent with the values used in our simulation. The undulatory evolution of a group of fibers is inside a network of fascicles and is not associated to a certain fascicle in general along the whole length of the trunk. This means that the

assumption that the fascicle is within a cylinder with constant radius is not valid in practice, but can be approximated on the trunk segment between two consecutive plexuses.

Another inconsistency of our simplified model is that inside the nerve trunk there is no synchronous undulation of all fascicles so in reality the compound action potential would result as a summation of action potentials generated along fascicular paths of different amplitudes, phases, and wavelengths. However, the influence of the inhomogeneities inside the nerve trunk, given by the fascicular structure, is less likely to contribute to stimulation due to the regularity in the stimulation sites found experimentally [25].

The analysis of the influence of the transverse field on nerve trunk stimulation was performed through the activating function of the passive model of the cable equation [34]. The linear relation of the activating function with the transmembrane voltage adequately describes the subthreshold behavior. One step further in the degree of complexity of the present model, the dynamic behavior of the membrane must be considered. The collision of the action potentials, initiated at the location of the virtual cathodes, along the fiber may influence the shape of the resulting compound action potential, upon which the judgment of multiple stimulation sites is made.

4. CONCLUSION

The present simulation study, according to the experimental observations [25], suggests that the electric field transverse to the nerve trunk can activate a nerve fiber within a fascicle through the field projection on fiber path determined by the fascicle undulation. Hence, the site of activation and stimulation threshold can be predicted using the longitudinal field activation mechanism and they are dependent on the wavelength and amplitude of the fascicle undulation. An induced electric field with both components, longitudinal and transverse to the nerve trunk, leads to a stimulation process characterized by the summation of effects produced individually by each component. Consequently, the presence of a transverse field component additional to the longitudinal field along the nerve trunk can determine variations in the stimulation threshold and the stimulation site as predicted by the classic cable theory based on the longitudinal field activation mechanism. Stimulation with an induced electric field transverse to the nerve trunk is characterized by a higher threshold and a compound action potential with multiple peaks (1 to 3 peaks

typical for a range of fascicle undulation wavelengths from 40 to 90 mm) as compared with stimulation with a longitudinal field.

REFERENCES

[1] Basser PJ, Roth BJ. Stimulation of myelinated nerve axon by electromagnetic induction. Med Biol Eng Comput. 1991; 29:261-268.

[2] Esselle KP, Stuchly MA. Neural stimulation with magnetic fields: analysis of induced electric fields. IEEE Trans Biomed Eng 1992; 39: 693-700.

[3] McNeal DR. Analysis of a model for excitation of myelinated nerve. IEEE Trans Biomed Eng 1976; 23(4): 329-337.

[4] Nagarajan SS, Durand DM. A generalized cable equation for magnetic stimulation of axons. IEEE Trans Biomed Eng 1996; 43(3): 304-312.

[5] Reilly JP. Peripheral nerve stimulation by induced electric currents: Exposure to time-varying magnetic fields. Med Biol Eng Comput 1989; 27:101-110.

[6] Roth BJ, Basser PJ. A model of the stimulation of a nerve fiber by electromagnetic induction. IEEE Trans Biomed Eng 1990; 37: 588-597.

[7] Roth BJ, Cohen LG, Hallett M, Friauf W, Basser PJ. A theoretical calculation of the electric field induced by magnetic stimulation of a peripheral nerve. Muscle Nerve 1990; 13: 734-74.

[8] Ruohonen J, Ravazzani P, Grandori F. An analytical model to predict the electric field and excitation zones due to magnetic stimulation of peripheral nerves. IEEE Trans Biomed Eng 1995; 42: 158-16.

[9] Veltink PH, van Veen BK, Struijk JJ, Holsheimer J, Boom HBK. A modeling study of nerve fascicle stimulation. IEEE Trans Biomed Eng 1989; 36(7): 683-691.

[10] Hsu KH, Durand DM. Prediction of neural excitation during magnetic stimulation using passive cable models. IEEE Trans Biomed Eng 2000; 47(4): 463-471.

[11] Nagarajan SS, Durand DM, Hsuing-Hsu K. Mapping location of excitation during magnetic stimulation: effects of coil position. Ann Biomed Eng 1997; 25: 112-125.

[12] Nilsson J, Panizza M, Roth BJ, Basser PJ, Cohen LG, Caruso G, Hallett M. Determining the site of stimulation during magnetic stimulation of peripheral nerve. Electroencephal Clin Neurophysiol 1992; 85: 253-264.

[13] Ruohonen J, Panizza M, Nilsson J, Ravazzani P, Grandori F, Tognola G. Transverse-field activation mechanism in magnetic stimulation of peripheral nerves. Electroencephal Clin Neurophys 1996; 101: 167-174.

[14] Krassowska W, Neu JC. Response of a single cell to an external electric field. Biophys J 1994; 66: 1768-1776.

[15] Plonsey R, Altman KW. Electrical stimulation of excitable cells – a model approach. Proc IEEE 1988; 76(9): 1122-1128.

[16] Friede RL, Meier T, Diem M. How is the exact length of an internode determined. J Neurol Sci 1981; 50: 217-228.

[17] Haninec P. Undulating course of nerve fibers and bands of Fontana in peripheral nerves of the rat. Anat Embryol 1986; 174: 407-411.

[18] Zachary LS, Dellon ES, Nicholas EM, Dellon AL. The structural basis of Felice Fontana's spiral bands and their relationship to nerve injury. J Reconstr Microsurg 1993; 9: 131-138.

[19] Schnabel V, Struijk JJ. Magnetic and electrical stimulation of undulating nerve fibers: a simulation study. Med. Biol. Eng. Comput. 1999; 37: 704-709,.

[20] Schnabel V. Mathematical models for magnetic stimulation of peripheral nerves. Ph.D. Thesis. Center for Sensory-Motor Interaction, Aalborg University, Denmark, 2001.

[21] Struijk JJ, Durand DM. Magnetic peripheral nerve stimulation: Axial versus transverse fields. Proceedings of the first joint BMES/EMBS conference, Atlanta, 1999; pp 469.

[22] Kobayashi M, Ueno S, Kurokawa T. Importance of soft tissue inhomogeneity in magnetic peripheral nerve stimulation. Electroencephalogr. Clin. Neurophysiol. 1997; 105(5): 406-413.

[23] Abdeen MA, Stuchly MA. Modeling of magnetic field stimulation of bent neurons. IEEE Trans. Biomed. Eng. 1994; 41(11): 1092-1095.

[24] Maccabee PJ, Amassian VE, Eberle LP, Cracco RQ. Magnetic coil stimulation of straight and bent amphibian and mammalian peripheral nerve in vitro: locus of excitation. J. Physiol. 1993; 460: 201-219.

[25] Lontis ER, Nielsen K, Struijk JJ. *In vitro* magnetic stimulation of pig phrenic nerve with transverse and longitudinal induced electric fields: analysis of the stimulation site. IEEE Trans. Biomed. Eng. 2009; 56(2): 500-512.

[26] Sunderland S. Nerves and Nerve Injuries. Churchill Livingstone, New York 1978.

[27] Plonsey R, Heppner DB. Considerations of quasi-stationarity in electrophysiological systems. Bul. Mathem. Biophys. 1967; 29: 657-664.

[28] Nagarajan SS, Durand DM, Warman EN. Effects of induced electric fields on finite neuronal structure: a simulation study. IEEE Trans. Biomed. Eng. 1993; 40: 1175-1188.

[29] Nagarajan SS, Durand DM, Roth BJ, Wijesinghe RS. Magnetic stimulation of axons in a nerve bundle: effects of current redistribution in the bundle. Ann. Biomed. Eng. 1995; 23: 116-126.

[30] Nagarajan SS Durand DM. Analysis of magnetic stimulation of a concentric axon in a nerve bundle. IEEE Trans. Biomed. Eng. 1995; 42: 926-933.

[31] Ruohonen J, Ravazzani P, Nilsson J, Panizza M, Grandori F, Tognola G. A volume-conductor analysis of a magnetic stimulation of peripheral nerves. IEEE Trans. Biomed. Eng. 1996; 43 : 669-678.

[32] Clarke E, Bearn JG. The spiral nerve bands of Fontana. Brain 1972; 95: 1-20.

[33] Pourmand R, Ochs S, Jersild RA. The relation of the beading of myelinated nerve fibers to the bands of Fontana. Neurosci. 1994; 61(2): 373-380.

[34] Schnabel V, Struijk JJ. Evaluation of the cable model for electrical stimulation of unmyelinated nerve fibers. IEEE Trans. Biomed. Eng. 2001; 48(9): 1027-1033.